Journal of Applied Fluid Mechanics, Vol. 11, No. 4, pp. 861-875, 2018.
Available online at www.jafmonline.net, ISSN 1735-3572, EISSN 1735-3645.
DOI: 10.29252/jafm.11.04.28559

Effects of Gas Cross-over through the Membrane on Water Management in the Cathode and Anode Sides of PEM Fuel Cell

K. Mohammadzadeh[1], H. Khaleghi[1†], H. R. Khadem Abolfazli[1] and M. Seddiq[2]

[1]*Department of Mechanical Engineering, Tarbiat Modares University, Tehran, 14115-111, Iran.*
[2] *School of Mathematical and Computer Sciences, Heriot-Watt University, Edinburgh, EH14 4AS, United Kingdom*

†*Corresponding Author Email: khaleghi@modares.ac.ir*

(Received September 1, 2017; accepted January 29, 2018)

ABSTRACT

Water management in a proton exchange membrane fuel cell (PEMFC) is numerically modeled by considering the 2D, non-isothermal steady flow assumptions. Governing equations are solved in all cell layers including cathode and anode electrodes by finite volume method using a single-region approach. The effect of gas cross-over through the membrane is studied on cell performance. This consideration, not only improves the general accuracy of modeling but also makes it possible to model energy losses due to direct reaction of reactant gases. The effect of some key variables such as liquid water diffusivity, current density, membrane thickness, etc. on PEMFC conditions such as the amount of saturated liquid water, power density, cell temperature, cross-over efficiency and so on are examined. It was observed that the amount of saturated liquid water on the anode side is considerably important. This observation addresses needs for further investigation of liquid water behavior in the anode electrode. The amount of liquid water saturation in both the cathode and anode electrodes is increased with increasing the current density. The results showed that at the current density of 0.2 A/cm2, cross-over effect causes about 10% reduction in cell efficiency and by decreasing the current density this effect is enhanced.

Keywords: Numerical investigation; PEMFC; Water Management at the anode; Gas cross-over through the membrane.

NOMENCLATURE

A	catalyst surface area per catalyst layer volume	φ	potential
a	water activity	ψ	liquid–vapor mass transfer coefficient
C	concentration	**Subscripts**	
D	diffusivity coefficient	a	anode
E^0	open circuit potential	act	activation
F	Farraday's constant	C	carbon
$\dot{G}$	mass flux	c	cathode
g	acceleration of gravity	cat	catalyst
H	Henry's law constant	CV	Control volume
h_{fg}	enthalpy of vaporization	d	index for electrodes (anode: d=a, cathode: d=c)
h_m	water vapor/dissolved water mass transfer coefficient	Dar	Darcy pressure loss
h_{react}	enthalpy of formation of water	DR	direct reaction
i	local current density	e	electrical
j	transfer current density	eff	effective
k	thermal conductivity	eod	electro-osmotic drag
K_L	liquid water permeability	f	fluid
L	length	gdl	gas diffusion layer

M	molar weight
n_{eod}	electro-osmotic drag coefficient
P	pressure
P_{atm}	atmosphere pressure
R	gas constant
RH	inlet relative humidity
r_m	radius of curvature
S	source term
$S^0_{f,a}$	entropy of reaction
s	liquid water saturation/entropy
Su	non-homogeneous generation term
T	temperature
t	thickness
u	velocity in x-direction
V	volume/cell voltage
v	velocity in y-direction
w	mass fraction
X	concentration (mole fraction)
α	charge transfer coefficient
Γ	surface tension
γ	switch function
ε	porosity or volume fraction
ζ_{imp}	impermeability efficiency
κ	gas permeability
μ	viscosity
ρ	density
σ	ionic conductivity
τ_{gdl}	GDL tortuosity

i	ionic
k	species (hydrogen, oxygen, water or nitrogen)
LV	mass transfer from liquid to vapor
m	membrane
ohm	ohmic
p	polymer
pc	phase change
ref	reference
rev	reversible heat
s	solid media
sat	saturated
th	theoretical
tot	total
w	water
WD	water dissolved in polymer
WV	water vapor
WL	water liquid
WP	water production

Superscripts

ave	average
c	critical
cp	capillary pores
cr	cross-over
D	diffusion
g	gas phase
L	liquid phase
p	polymer phase

1- INTRODUCTION

Nowadays, fuel cells and especially proton exchange membrane fuel cells (PEMFCs) have been receiving great attention in the researches as an alternative technology for energy storage which is more environmentally friendly and efficient compared to fossil fuel technologies (Rajan *et al*. 2018).

In PEMFC, when the membrane humidity is low, the ionic conductivity of the membrane will decrease. As a result, the output energy will decrease (it is called dehydration which results in the rupture of membrane). On the other hand, extra water in PEMFC might block (Gas Diffusion Layer) GDL holes, that will prevent catalyst layer (CL) from receiving reactant gas (this phenomenon is called flooding, and it causes an increase in concentration potential loss). Due to the aforementioned reasons, a good PEMFC performance is a function of good water management. Water can be condensed from the inlet gas into the gas flow channel (GFC) due to decreasing of operating temperatures, increasing of pressure, or increasing of the moisture in the gas. Water in the liquid phase can be transported within the GDL and CL via capillary action. Water flow between the cathode and the anode takes place by three mechanisms: electro-osmotic drag, back diffusion, and pressure driven flow.

In the early studies on the PEMFC, effect of liquid water was ignored (one-dimensional models of Springer *et al.* (1991) and Bernardi and Verbrugge (1992), two-dimensional models of Gurau *et al.* (1998), Um, *et al.* (2000) and Siegel *et al.* (2003)). However, over the past two decades, many numerical works were done for investigation on water management.

Natarajan and Van Nguyen (2001) presented a two-dimensional, perpendicular to the GFC direction, transient, two-phase and multi-component model for considering the liquid water transfer in GDL. It is assumed that liquid water movement occurs due to capillary pressure and also mass transfer between liquid and vapor phases is possible. The relation between capillary pressure and water saturation is presented based on PEMFC test data. They showed that their correlation is somehow different from Leveret common function.

Pasaogullari and Wang (2004) compared two different two-phase flow modeling techniques in GDL including the UFT method and the M2 method. The flow due to capillary pressure, especially in two-phase systems with low liquid saturation, is effective in the amount of water saturation and oxygen concentration. Pasaogullari (2005), in his doctoral thesis, focused on the effect of water transferred in the GDL on modeling the two-phase flow and flooding in PEMFC under different working conditions. His results showed that water transfer in the GDL is strongly temperature dependent.

Seddiq *et al*. in 2006 presented a unified two dimensional (vertical to GFC direction) and steady-state model for PEMFC. In their model, it is assumed that reactant gases are dissolved in membrane water and then transferred to the other side where the diffusive gas causes a direct reaction and produces water (the formation of liquid water is not considered). In their study, the effect of cross-

over phenomenon on the cell efficiency is considered as a loss factor. The results showed that this effect is not always negligible especially in the calculation of cell efficiency and in some cases, the phenomenon of cross-over effect on the efficiency of the cell is approximately 2%.

Hwang (2007) developed a complete two-phase model (Two-fluid model) including fluid flow, heat transfer, and electric current for a porous PEMFC cathode. The main feature of their model was the successful prediction of the equilibrium front of the phases and also the thermal equilibrium front in the porous cathode which leads to more realistic spatial variations of the two-phase parameters.

Simulation of water management in recent years has been investigated from various aspects (Cai *et al*. 2016; Anderson *et al*. 2016; Zhang *et al*. 2017 and Ashrafi and shams, 2017) and functional strategies have been proposed.

As is seen in the review papers in the PEMFC modeling (Anderson *et al.* 2010; Djilali 2007; Ferreira *et al.* 2015; Siegel 2008; Song and Meng 2013; Weber *et al.* 2014), the main focus of the water management studies has been on the cathode side. The main reason for this is that the cathode electrode is a water producer and is where the likelihood of flooding is much higher. However, experimental studies revealed that flooding can also be observed in the anode GFC for special working conditions and it can be even more notable than the cathode side (Ge and Wang 2007; Lee and Bae 2012; Sergi and Kandlikar 2011). The mechanism for the formation of liquid water as well as flow rate, properties of gas in the anode GFC were different from those observed on the cathode side. Therefore, the behavior of liquid water in two electrodes might be very different which needs different water management techniques. To the best of the authors' knowledge, a few numerical studies have been published in the field of anode water management which we reviewed them here.

The first study of the two-phase flow in an anode GFC of a PEMFC is the work of Ferreira *et al*. in 2015 which was a numerical investigation using VOF (Volume Of Fluid). In this study, the flow was assumed to be laminar, isothermal and transient, and phase-change and gravity effects were ignored and the electrochemical reactions inside the PEMFC were not considered. 3D simulations have been done by using Fluent software and finally liquid water distribution in the GFC was obtained.

Xing *et al.* (2016) described a steady, non-isothermal and two-dimensional along-the-channel CFD model coupled with a two-phase flow model of liquid water and gas transport for a PEMFC (Xing *et al*. 2016). In this study, liquid water saturation was simulated inside the electrodes and channels at both the anode and cathode sides. Three types of models were compared for the catalyst layers. Their results showed that the chance of water flooding, represented by liquid water saturation, is higher near the downstream channel of both the anode and cathode.

Hou *et al.* (2017) simulated the gas-liquid two-phase flow of low-temperature fuel cells to study the water removal process in the anode channel utilizing VOF method .It is found that the water removal process in the cathode channel is easier compared to the same process that occurs in the anode under the same operating condition and inlet velocity. Increasing the humidification rate and the contact angle is helpful for water removal.

Water management simulation in PEMFC is critical, and there are a lot of studies in this field which some of the most recent ones have been mentioned above, but the models developed so far have not considered the effect of gas cross-over through the membrane, and they have mostly focused on the cathode electrode. In the present paper, two-phase water transport is included in the model both in cathode and anode, and its effect in the presence of gas cross-over through the membrane has been examined carefully.

2. PROBLEM STATEMENT

In this paper, a two-dimensional, steady state and non-isothermal model in the GFC direction is presented (Fig. 1). Water in the cell is considered to be in the form of vapor, liquid and dissolved phase in the form of the polymer. A transport equation for liquid water saturation is solved throughout the cell for modeling the water management. The main approach in this model is single-region. So, all transfer terms are solved in all PEMFC parts. Equations form can be changed from one layer to another. For example, in the GFC, the momentum equation is in the form of the Navier-Stokes equation, but in GDL and CL, it reduced to the Darcy equation. In this paper, the effects of liquid water transfer and cross-over phenomenon along with the effect of several key variables such as liquid water diffusivity, current density, membrane thickness and the ratio of O_2 to N_2 on PEMFC performance have been investigated, and the results are presented and discussed.

3. GOVERNING EQUATIONS

In all layers, the flow is assumed 2D, steady state, non-isothermal, laminar and incompressible with variable density. The main equations are mass, momentum, species (oxygen and water vapor), liquid water, proton and energy conservation which are solved in all PEMFC parts using a single-region approach. Governing equations for different layers are summarized in Table 1. Subsidiary equations for physical and electrochemical properties are also presented in Tables 6 and 7. Media is of the porous type in all areas except for GFCs. Porosity modeling in the equations is applied by defining porosity coefficient ε.

3.1. Gas Flow Channels

Mixture density is derived based on ideal gas equation (Eq. (1)), coupled to gaseous species

Table 1 Governing equations

GFC	
Continuity	$\nabla\cdot[\varepsilon(\rho^g\vec{u}+G^{\bullet D})]=S_{LV}$ $G^{\bullet D}=\sum_k -D_k\nabla X_k\rho_k$
Momentum	$\nabla\cdot(\varepsilon\rho\vec{u}\vec{u})=-\varepsilon\nabla P+\nabla\cdot(\varepsilon\mu_{eff}\nabla\vec{u})$
Water vapor at anode side	$\varepsilon\rho^g\vec{u}\cdot\nabla w_{WV}+w_{WV}\nabla\cdot(\varepsilon\rho^g\vec{u})$ $=\nabla\cdot(D^g_{WV}\rho^g\nabla w_{WV})+S_{LV}$
Oxygen at cathode side	$\varepsilon\rho^g\vec{u}\cdot\nabla w_{O2}+w_{O2}\nabla\cdot(\varepsilon\rho^g\vec{u})$ $=\nabla\cdot(D^g_{O2}\rho^g\nabla w_{O2})$
Water saturation	$\varepsilon\vec{u}\cdot\nabla s=\nabla\cdot(D^{cp}_{WL}\nabla s)-(S_{LV}/\rho_{WL})$
Energy	$(\varepsilon\rho^g C_{eff})\vec{u}\cdot\nabla T=\nabla\cdot(K_{eff}\nabla T)-S_{LV}h_{fg}$
GDL	
Continuity	$\nabla\cdot[\varepsilon(\rho^g\vec{u}+G^{\bullet D})]=S_{LV}$ $G^{\bullet D}=\sum_k -D_k\nabla X_k\rho_k$
Momentum	$\frac{\partial P}{\partial y}=\frac{-\varepsilon\mu}{\kappa}u_y,\quad \frac{\partial P}{\partial x}=\frac{-\varepsilon\mu}{\kappa}u_x$
Water vapor at anode side	$\varepsilon\rho^g\vec{u}\cdot\nabla w_{WV}+w_{WV}\nabla\cdot(\varepsilon\rho^g\vec{u})$ $=\nabla\cdot(D^g_{WV}\rho^g\nabla w_{WV})+S_{LV}$
Oxygen at cathode side	$\varepsilon\rho^g\vec{u}\cdot\nabla w_{O2}+w_{O2}\nabla\cdot(\varepsilon\rho^g\vec{u})$ $=\nabla\cdot(D^g_{O2}\rho^g\nabla w_{O2})$
Water saturation	$\nabla\cdot(D^{cp}_{WL}\nabla s)-S_{LV}/\rho_{WL}=0$
Energy	$(\varepsilon\rho^g C_{eff})\vec{u}\cdot\nabla T=\nabla\cdot(K_{eff}\nabla T)+S_{pc}$ $S_{pc}=-S_{LV}h_{fg}$
CL	
Continuity	$\nabla\cdot[\varepsilon(\rho^g\vec{u}+G^{\bullet D})]=S_{H2}+S_{O2}$ $+S_{LV}+S_{WP}\gamma_{LV}-S_{WD}\gamma_{WD}$ $+S_{eod}\rho_{WD}-Su^s-Su^{DR}$
Momentum	$\frac{\partial P}{\partial y}=\frac{-\varepsilon\mu}{\kappa}u_y,\frac{\partial P}{\partial x}=\frac{-\varepsilon\mu}{\kappa}u_x,\kappa_{CL}=\kappa_{GDL}$
Water vapor at anode side	$\varepsilon\rho^g\vec{u}\nabla w_{WV}+w_{WV}\nabla\cdot(\varepsilon\rho^g\vec{u})$ $=\nabla\cdot(D^g_{WV}\rho^g\nabla w_{WV})+S_{LV}$ $+S_{WP}\gamma_{LV}-S_{WD}\gamma_{WD}+Su^{DR}$
Oxygen at cathode side	$\varepsilon\rho^g\vec{u}\nabla w_{O2}+w_{O2}\nabla\cdot(\varepsilon\rho^g\vec{u})$ $=\nabla\cdot(D^g_{O2}\rho^g\nabla w_{O2})+S_{O2}-Su^s-Su^{DR}$
Water saturation	$\nabla\cdot(D^{cp}_{WL}\nabla s)-S_{LV}/\rho_{WL}+S_{WP}(1-\gamma_{LV})/\rho_{WL}$ $-S_{WD}(1-\gamma_{WD})/\rho_{WL}=0$
Ion(proton)	$\nabla\cdot(\sigma_{i,eff}\nabla\phi_i)+S_i=0,\quad S_i=R_{eff}$
Energy	$(\varepsilon\rho^g C_{eff})\vec{u}\cdot\nabla T=\nabla\cdot(K_{eff}\nabla T)$ $+S_{ohm}+S_{rev}+S_{act}+S_{pc}+S_{DR}$
Membrane	
Ion(proton)	$\nabla\cdot(\sigma_i\nabla\phi_i)=0$
Energy	$\nabla\cdot(k_{eff}\nabla T)=S_{ohm},\quad k_{eff}=k_p$

equations. Porosity coefficient at GFCs is equal to 1, and it is assumed that liquid water is transferred by drops (convection mechanism) that are of negligible volume and have an equal speed to gas flow. *S* parameter is water saturation that is defined in porous media as the ratio of total liquid volume to nonsolid volume in the control volume. S_{LV} is production term (mass flux variation due to evaporation and condensation of water liquid) which is used in continuity equation of gas phase and species conservation for water. S_{LV} is defined as Eq. (2).

$$\rho^g=C_{tot}\sum_k X_k M_k\ ,\ C_{tot}=P/RT \tag{1}$$

$$S_{LV}=\psi s\gamma_{LV}-\psi(1-s)(1-\gamma_{LV}) \tag{2}$$

$$\gamma_{LV}=1-0.5[1+\tanh(C_1(\rho^g_{WV}/\rho^g_{sat})-C_2)] \tag{3}$$

Experimental data does not exist for ψ, thus should be chosen so large that local equilibrium is established between the vapor and liquid phases. If in Eq. (2) γ_{LV}=1, then evaporation will occur. On the other hand, if γ_{LV}=0, condensation phenomenon will occur. The idea of using key function γ_{LV} (see Eq. (3)), in vapor-liquid water phase change has been used in previous studies (Meng 2007; Natarajan and Van Nguyen 2001; Siegel *et al.* 2004). By defining C_1 and C_2 values, γ_{LV} variation rate can be controlled between 0 and 1. Here, C_1=61 and C_2=59 (Siegel *et al.* 2004). Due to these values, when local relative humidity is below 98%, evaporation will occur while condensation will occur at a higher rate. Generation term at the end of energy equation shows that the heat transfer is related to water condensation and evaporation.

3.2 Gas Diffusion Layer

Equations of Mass and gas species conservation is identical with GFC and will not be presented here again. Linear momentum conservation equation in the porous region is in the form of Darcy equation. Capillary pressure (P^c) which drives water liquid to the gaseous dry region, can be defined by $P^c=P^g-P^L=2\Gamma/r_m$ (Siegel *et al.* 2003). Liquid water capillary diffusivity is defined as Eqs. (4) and (5) (Natarajan and Van Nguyen 2001).

$$D^{cp}_{WL}=(\rho_{WL}g/\mu_{WL})K_L(s)(\partial P_c/\partial s) \tag{4}$$

$$K_L(s)\partial P_c/\partial s=0.0155s^3-0.0213s^2+0.0088s+0.0002 \tag{5}$$

Generation term S_{LV} is used for calculating mass transfer rate between gaseous and liquid phases in Eq. (2). GDL permeability $K_L(s)$ is considered as an approximate parameter. The usage of a precise approximation gives correspondent results with

experimental results. Generation term S_{pc} in energy equation is for calculating phase change Energy.

3.3 Catalyst Layer

Mass transfer coefficients ψ and h_m in Eq. (6) must be considered large enough, in order to reach equilibrium between liquid, dissolved and gaseous phases. S_{eod} is the generation term which is related to electro-osmotic drag. Generation terms Su^s (solution of gas species in water liquid) and Su^{DR} (direct reaction) are described in Seddiq (2006) completely.

$$\begin{aligned} &S_{H2}=\frac{-M_{H2}}{2F}\left|R_{eff,a}\right|, \quad S_{O2}=\frac{-M_{O2}}{4F}\left|R_{eff,c}\right|, \\ &S_{WP}=\frac{M_W}{2F}\left|R_{eff,c}\right|, \quad S_{WD}=h_m(\rho_{WV}^g-\rho_{WV}^p), \\ &S_{eod}=-\frac{\nabla\vec{in}^{eod}}{FC_{tot}}, \quad \rho_{WD}=M_wC_{tot} \end{aligned} \tag{6}$$

Effective reaction rate, R_d is based on Bulter-Volmer equation, on which some modifications have been done (Eq. (7)). R_d is controlled by the concentration of reactants in the polymer, local activation potential $(\phi_{e,d}-\phi_i)$, reaction exchange, current density, and catalyst area. When liquid water fills the pores, access path of reactant gases to CL region is blocked, and it will result in a decrease in accessible reaction area and reaction rate. R_d is actually transfer current density (j).

$$\begin{aligned} R_d=&(1-s)Ai_{0,k}\left(\frac{C_k^p}{C_{k,ref}}\right)^{\gamma} \\ &\times\left[\exp((\phi_{e,d}-\phi_i)\alpha_d\frac{n_dF}{RT}\right) \\ &-\exp(-(\phi_{e,d}-\phi_i)\alpha_d\frac{n_dF}{RT})] \end{aligned} \tag{7}$$

Reactants concentration in the reaction zone is achieved by Henry's law, which defines the concentration of reactant gases in the dissolved phase in the interface of gas and polymer (see Eq. (8), Siegel 2003).

$$C_k^p=h_k^pC_k^pT \tag{8}$$

It is assumed that electrical potential in each CL and GDL electrode is constant. As it is shown in Eq. (9), electrical potential in the anode is set to zero and in the cathode is assigned as negative of the total over-potential (Siegel 2003).

$$\phi_{e,a}=0\ ,\ \phi_{e,c}=-(E_{th}-V_{cell}) \tag{9}$$

Mass transfer between gaseous and dissolved phases is defined by S_{WD} (see Eq. (7)), which works with key function γ_{WD} (see Eq. (10)). When the density of the water vapor in equilibrium with the polymer is lower than local vapor density $(\rho_{WV}^p<\rho_{WV}^g)$, γ_{WD} is equal to one, which shows that water vapor converts to polymer phase or dissolved phase. Water density in equilibrium with a polymer, is a function of local water activity a. Due to initial assumption, water in dissolved phase, can only be converted to the liquid phase, and in that phase, it can be stayed in the liquid phase or be vaporized (Siegel 2003).

$$\begin{aligned} &\gamma_{WD}=0.5+\left(\rho_{WV}^g-\rho_{WV}^p\right)\Big/\left(2\times\left|\rho_{WV}^g-\rho_{WV}^p\right|\right), \\ &\rho_{WV}^p=\rho_{sat}^g\cdot a, \quad \rho_{WV}^g=w_{WV}\cdot\rho^g \end{aligned} \tag{10}$$

Generation terms in the equation of liquid water transfer include mass transfer between liquid and gaseous phase, liquid and dissolved phase and water production because of the electrochemical reaction. These generation terms similar to mass conservation, only permit one-directional mass transfer from the dissolved phase to the liquid phase and after that, liquid water may remain liquid or evaporate, depending on local relative humidity. Generation term S_i shows the rate of proton production in the anode and its consumption in the cathode. The integral of S_i is equal on the both of anode and cathode sides; that is all protons which are generated at the anode and are consumed at the cathode. The current density i_i is calculated based on Eq. (11).

$$\begin{aligned} &i_i=\sigma_{i,eff}\nabla\phi_i, \quad \sigma_{i,eff}=\sigma_i\varepsilon_p, \\ &\sigma_i=f(\lambda,T)=(0.5139\lambda-0.326)\times \\ &\exp[1268.0(\frac{1}{303}-\frac{1}{T})] \end{aligned} \tag{11}$$

The generation terms of energy conservation equation in CLs are different from GDL (Eq. (12)). G^{cr} is the flux of water production in direct reaction. The enthalpy of dissolved water is considered to be equal to that of water liquid.

$$\begin{aligned} &S_{rev}=\frac{R_{eff,k}T}{n_kF}\sum_{p-r}S_f^0 \\ &S_{ohm}=\sigma_{i,eff}(\nabla\phi_i\cdot\nabla\phi_i)=i^2\big/\sigma_{i,eff} \\ &S_{pc}=(-S_{LV}+S_{DW}\gamma_{DW})h_{fg} \\ &S_{DR}=G^{\bullet cr}h_{react} \\ &S_{act}=(\phi_e-\phi_i)R_{eff} \end{aligned} \tag{12}$$

3.4 Membrane

Proton and energy transfer in the membrane is done only by diffusion. The proton conductivity of Nafion, σ_i based on Springer *et al.* (1991), is written in Eq. (11). Current density is calculated by Eq. (13).

$$i_i=\sigma_i\nabla\phi_i \tag{13}$$

3.5 Boundary Conditions

The computer code for solution domain (as shown

Table 2 Boundary conditions of governing equations

Type of equation	Boundary 1	Boundary 2	Boundary 3	Boundary 4	Boundary 5	Boundary 6	Boundary 7	Boundary 8
Continuity (P)	$P'=0$	$P'=0$	$P=a$	$P=P_c$	---	---	$\frac{\partial P}{\partial y}=0$	$\frac{\partial P}{\partial y}=0$
Momentum (u)	$u=0$	$u=0$	$u=0$	$u=0$	$\frac{\partial u}{\partial y}=0$	$\frac{\partial u}{\partial y}=0$	$\frac{\partial u}{\partial y}=0$	$\frac{\partial u}{\partial y}=0$
Momentum (v)	$v=0$	$v=0$	$v=1.547\ m/s$	$v=3.747\ m/s$	$\frac{\partial v}{\partial y}=0$	$\frac{\partial v}{\partial y}=0$	$\frac{\partial v}{\partial y}=0$	$\frac{\partial v}{\partial y}=0$
Oxygen species	$\frac{\partial X_{o_2}}{\partial x}=0$	$\frac{\partial X_{o_2}}{\partial x}=0$	$X_{O_2}=0$	$X_{O_2}=(1-X_w)\frac{R_{O\text{-}N}}{1+R_{O\text{-}N}}$	$\frac{\partial X_{o_2}}{\partial y}=0$	$\frac{\partial X_{o_2}}{\partial y}=0$	$\frac{\partial X_{o_2}}{\partial y}=0$	$\frac{\partial X_{o_2}}{\partial y}=0$
Water vapor species	$\frac{\partial X_{WV}}{\partial x}=0$	$\frac{\partial X_{WV}}{\partial x}=0$	$X_{WV}=\frac{RH_a\cdot P_{sat}}{P}$	$X_{WV}=\frac{RH_c\cdot P_{sat}}{P}$	$\frac{\partial X_{WV}}{\partial y}=0$	$\frac{\partial X_{WV}}{\partial y}=0$	$\frac{\partial X_{WV}}{\partial y}=0$	$\frac{\partial X_{WV}}{\partial y}=0$
Saturation (liquid water)	$\frac{\partial s}{\partial x}=0$	$\frac{\partial s}{\partial x}=0$	$s=0$	$s=0$	$\frac{\partial s}{\partial y}=0$	$\frac{\partial s}{\partial y}=0$	$\frac{\partial s}{\partial y}=0$	$\frac{\partial s}{\partial y}=0$
Energy	$T=353^\circ K$	$T=353^\circ K$	$T=353^\circ K$	$T=353^\circ K$	---	---	---	---
Phase potential	Boundary conditions on the boundary of CL, is set to $\frac{\partial \phi}{\partial x}=0$						$\frac{\partial \phi}{\partial y}=0$	$\frac{\partial \phi}{\partial y}=0$

in Fig. 1) is programmed and modeled. In order to show the boundary conditions, eight regions are shown in this model. Boundary conditions are shown in Table 2.

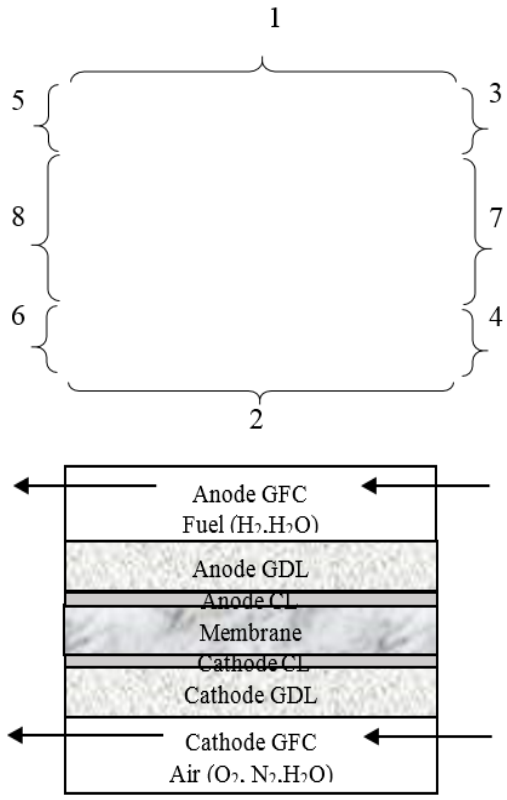

Fig. 1. Boundaries of computational domain

4. ELECTROCHEMICAL QUANTITIES

The relations used for calculating electrochemical quantities are summarized in Table 3. Potential difference for two sides of the cell is calculated by $V^{cell}=E^0-(V^{ohm}+V_a^{act}+V_c^{act})$.

Table 3 Electrochemical quantities relations

Quantity	Relation
Open circuit voltage (Hu *et al*. 2004)	$E^0=1.229-0.83e^{-3}(T-298.15)+4.31e^{-5}TLn((\frac{P_{H2}}{P_{atm}})(\frac{P_{O2}}{P_{atm}})^{0.5})$
Activation over-potential	$V_a^{act}=\frac{RT}{F}\ln(\frac{i}{i_a^{ref}X_{H_2}(1-s)})$ $V_c^{act}=\frac{2RT}{F}\ln(\frac{i}{i_c^{ref}X_{O_2}(1-s)})$
Ohmic over-potential	$V^{ohm}=\int_a^c\frac{i_X}{\sigma}dx$
Transfer current density	$j=\nabla\vec{i}=\begin{cases}j_a: anode\ CL\\ j_c: cathode\ CL\\ 0: other\end{cases}$
Coefficient of electro-osmotic drag	$n_{eod}=0.0029\lambda^2+0.05\lambda-3.4\times10^{-19}$

5. PHYSICAL PROPERTIES

The relations related to physical properties are presented in Table 4. For each fluid μ_k is a function of temperature. In order to modify average viscosity in porous media, given equation for μ_{eff} is used (Seddiq *et al*. 2006).

Thermal conductivity in GFC, because of gas existence, is derived using average mole. k_{eff}, in GDL is obtained as a combination of averaged gaseous conductivity, porous media and liquid water

Table 4 Physical properties relations of PEMFC

Property	Relation
Average dynamic viscosity	$\mu=\frac{\rho_k\mu_k}{\rho}=\sum_k X_k M_k \mu_k \Big/ \sum_k X_k M_k$, $\mu_{eff}=\left[\frac{1.5(1-\varepsilon)}{\varepsilon}\right]^2\mu$, $0<\varepsilon<1$
Conductivity in GFC	$K_{eff}=\sum_k X_k K_k=\begin{cases} X_{O2}K_{O2}+X_{N2}K_{N2}+X_{H_2O}K^g_{H_2O}: GFC\ cathode \\ X_{H2}K_{H2}+X^g_{H_2O}K_{H_2O}: GFC\ anode \end{cases}$
Conductivity in GDL	$K_{eff}=\varepsilon_{gdl}(1-s)K_g+\varepsilon_{gdl}sK_{WL}+(1-\varepsilon_{gdl})K_c$, $K_g=\sum_k X_k K^g_k$
Conductivity in CL	$K_{eff}=\varepsilon_{cat}(1-s)K_g+\varepsilon_{cat}sK_{wl}+\varepsilon^c_{cat}K_c+\varepsilon^P_{cat}K_P$
Conductivity in Membrane	$K_{eff}=\varepsilon_{mem}K_g+(1-\varepsilon_{mem})K_P$
Effective heat capacity in GFC	$C_{eff}=\sum_k w^g_k C^g_k=\begin{cases} w_{O2}C_{O2}+w_{N2}C_{N2}+w^g_{H_2O}C^g_{H_2O}: GFC\ cathode \\ w_{H2}C_{H2}+w^g_{H_2O}C^g_{H_2O}: GFC\ anode \end{cases}$
Effective heat capacity in GDL and CL	$C_{eff}=C_g\varepsilon_{gdl}(1-s)+C_{wl}\varepsilon_{gdl}s+(1-\varepsilon)C_s$, $C_g=\sum_k C_k C^g_k$
Mass diffusivity	$GFC: D^g_k=D^{ref}_k\left(\frac{T}{T^{ref}}\right)^{1.5}\left(\frac{P^{ref}}{P}\right)$, $GDL: D^g_{k,eff}=D^g_k\frac{\varepsilon^{gdl}_{void}(1-s)}{\tau_{gdl}}$, $CL: D^g_{k,eff}=D^g_k[\varepsilon^{gdl}_{void}(1-s)]^{1.5}$
Mass diffusivity in membrane [11]	$D_{WD}=D_i e^{2416\left(\frac{1}{303}-\frac{1}{T}\right)}$, $D_i=\begin{cases} 10^{-10} & \lambda<2 \\ 10^{-10}(-3+2\lambda) & 2<\lambda\le 3 \\ 10^{-10}(6.5-1.167\lambda) & 3<\lambda\le 4.5 \\ 1.25\times10^{-10} & 4.5\le\lambda \end{cases}$
Water content in membrane	$\lambda=\begin{cases} 0.043+17.81\,a_w-39.85\,a_w^2+36.0\,a_w^3 & 0<a\le 1 \\ 14.0+1.4(a_w-1) & 1\le a\le 3 \\ 16.8 & 3<a \end{cases}$

(Seddiq *et al.* 2006). In CL, conductivity is a combination of gaseous, carbon, polymer and liquid parts. In the membrane polymer, conductivity is taken to be equal to its value for polymer ($K_{eff}=K_P$).

Effective heat capacity, C_{eff}, is calculated based on liquid and solid media. C_{eff}, in GDL and CL, is dependent on liquid water and C_s is heat capacity of the solid phase.

In regions that species are gas and insoluble like GFC, mass diffusivity follows the general form of the relationship presented in Table 4 (Seddiq *et al.* 2006). Due to the existence of solid and liquid water, there is a barrier to gas diffusion and so mass diffusivity for GDL and CL must be modified based on (Meng 2007). GDL might swell, due to pressure caused by PEMFC assembly which enters GFC and closes part of the GFC area. This phenomenon is modeled as a coefficient called

tortuosity in mass diffusivity ($\tau=\varepsilon^{1.5}$). Thickness and porosity in GDL are defined in a way that includes shape change due to GFC shoulder pressure. In the membrane, the species are in the dissolved phase. In this condition, mass diffusivity is a few orders lower than the free condition. Mass diffusivity, for hydrogen and oxygen is calculated using $D^s_k=CT/\mu$ (Seddiq *et al.* 2006), μ is the viscosity of the solution, C is a constant that is dependent on the dissolved material.

λ, is membrane water content and in Table 4 which is defined based on water activity $a_w=X_{water}P/P_{sat}$. water activity in the gaseous phase is equal to relative humidity. Saturation pressure P_{sat}, is calculated using Eq. (14) (Seddiq *et al.* 2006). The total mole of material per unit volume, in gaseous and liquid phase, is written in Eq. (15).

$$P_{sat}=9.5782e^{-4}T^4-1.07899812T^3+4.589572e^2T^2-8.7277445e^4T+6.2552433e^6 \quad (14)$$

$$\text{Gas phase}: C_{tot}=P/RT \qquad \text{Liquid phase}: C_{tot}=C_{water}/X_{water} \quad (15)$$

6. SCALING THE CROSS-OVER

As part of the contribution of the present paper to the study of the transfer of water in the PEMFC, this section introduces the phenomenon of the reactant gases cross-over in the loss of the cell efficiency.

Seddiq *et al.* (2006) expressed the amount of cross-over by using a cross-over equivalent current density, i^{cr} which is defined by Eq. (16). This variable shows the amount of electric current loss due to the direct reaction of hydrogen and oxygen in the anode and cathode sides (Seddiq *et al.* 2006).

$$i^{loss} = i_a^{loss} + i_c^{loss} = i^{ideal} - i^{ave}, \quad i_a^{loss} = 4F\dot{G}_{O_2}^{cr}, \quad i_c^{loss} = 2F\dot{G}_{H_2}^{cr} \tag{16}$$

Seddiq *et al.* (2006) introduced the overall impermeability efficiency as Eq. (17) in order to quantify the energy efficiency of the cell in terms of impermeability against reactant gases.

$$\xi^{imp} = 1 - \frac{i_a^{loss}}{i_a^{loss} + i^{ave}} - \frac{i_c^{loss}}{i_c^{loss} + i^{ave}} \tag{17}$$

Overall impermeability efficiency is taken into account as a multiplying factor to obtain the overall efficiency of the fuel cell (Seddiq *et al.* 2006).

7. NUMERICAL SIMULATION

Physical properties used in the simulation are shown in Table 5 and geometrical properties together with base cell operating conditions are illustrated in Table 6. In this paper, reference current density is considered as 1.18 Acm^{-2}, unless it is mentioned otherwise.

7.1 Numerical Domain and Grid

Dimensions for the computational domain and the number of meshes for each layer in the base case are shown in Table 7. Wherever there is a higher gradient, the size of the mesh is smaller. In this simulation, only one mesh is considered for CL. Two grid are used simultaneously, the main grid is used for scalars such as *T*, *P,* and *X*, and staggered grid is used for vectors such as *U*, *V*, i_x, and i_y.

Table 5 Physical properties

ρ_{wl} at 80 °C	971.82 Kgm^{-3}	h_{react} or h_{fg}	-285830 JKg^{-1}
α_a	0.50	R	8.314 $JKg^{-1}K^{-1}$
α_c	0.55	F	96487 $Cmol^{-1}$
$S^0_{f,a}$	42.5 $Jmol^{-1}K^{-1}$	D^{ref}_{H2}	1.1×10^{-4} m^2s^{-1}
$S^0_{f,c}$	126.8 (liquid water) 64.8 (water vapor)	D^{ref}_{O2}	3.2×10^{-5} m^2s^{-1}
$K_{hy,gdl}$	1.76×10^{-11} m^2	D^{ref}_{water}	7.35×10^{-5} m^2s^{-1}
$K_{hy,m}$	1.8×10^{-18} m^2	D^{s}_{H2} at 353 K	1.06×10^{-8} m^2s^{-1}
ρ_m	1840 Kgm^{-3}	M_{H2}	2.016×10^{-3} $Kgmol^{-1}$
M_m	1.1 $Kgmol^{-1}$	M_{O2}	31.999×10^{-3} $Kgmol^{-1}$
i^{ref}_a	100 Am^{-2}	M_W	18.015×10^{-3} $Kgmol^{-1}$
i^{ref}_c	1000 Am^{-2}	M_{N2}	28.013×10^{-3} $Kgmol^{-1}$
T^{ref}	353 K	K_{gdl}	0.231 $Jm^{-1}K^{-1}$
P^{ref}	101325 Pa	K_m,K_{cat}	0.147 $Jm^{-1}K^{-1}$

7.2 Numerical Solution Process

An in-house FORTRAN code is developed for solving the governing equations based on finite volume method in which power law scheme is used for solving all governing equations, and SIMPLE algorithm is used to overcome pressure-velocity coupling. Then, all equations are solved using line-by-line iteration, which employs a three diagonal matrix algorithm.

Table 6 Geometrical properties and operational conditions of the base cell

L_{cell}	2.0 mm	P_{in}	310 KPa
t_{GFC}	1.0 mm	RH_a	95%
$t_{GDL,a}$	0.290 mm	RH_c	95%
$t_{GDL,c}$	0.254 mm	τ_{gdl}	3.5
t_{CL}	0.0165 mm	$\Psi_{evap/cond}$	2000 $Kgm^{-3}s^{-1}$
t_m	0.0508 mm	h_m	5000 s^{-1}
ε^{gdl}_{void}	0.375	$T_{f,a}$	353 K
ε^{cat}_{C}	0.45	$T_{f,c}$	353 K
ε^{cat}_{void}	0.31	$R_{O2/N2}$ at cathode gas channel inlet	0.266
ε^{cat}_{p}	0.24		

Table 7 Dimensions of computational domain and grid size (the base case)

Membrane	Cathode CL	Anode CL	Cathode GDL	Anode GDL	Cathode GFC	Anode GFC	layer
0.0508	0.0165	0.0165	0.254	0.29	1.0	1.0	**Dimension in x direction** (mm)
2.0	2.0	2.0	2.0	2.0	2.0	2.0	**Dimension in y direction** (mm)
4	1	1	17	19	108	108	**number of meshes in x direction**
51	51	51	51	51	51	51	**number of meshes in y direction**

8. RESULTS AND DISCUSSIONS

8.1 Validation by Experimental Results

A mesh independent grid size of 260×51 is used in the calculations. The present model is a development of the model of Seddiq *et al.* 2006 which has already been validated by comparing to the experimental data of Wang *et al.* (2003) obtained in similar conditions. However, further verifications are carried out to validate the present model. In Fig. 2, the polarization curve of the present two-phase model is compared with experimental data of Siegel *et al.* (2004) which shows a satisfactory agreement between the numerical and experimental results. Experimental data has an error of ±0.025V in potential and ±0.02Acm^{-2} in current density. Thus the results obtained by the computational model are in the range of experimental data error.

In addition to the polarization curve, the predicted

location and value of the maximum saturation of the liquid water are also examined. The maximum saturation of the liquid water occurs at the vicinity

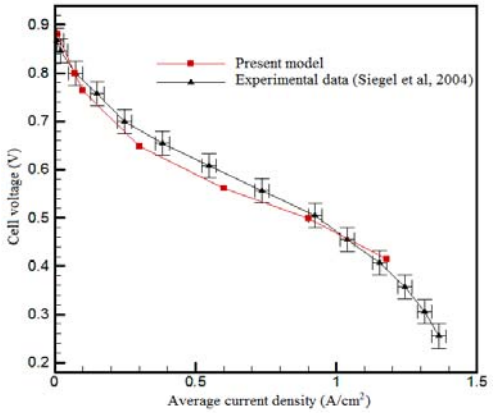

Fig. 2. Comparison between the model predictions and experimental data

of the catalyst close to the edge of the cell, and its value is predicted to be about 0.497 showing approximately 6% difference with that of Siegel *et al*. 2004 (≈0.469).

As the cross-over phenomenon is important in low current densities (Seddiq *et al*., 2006), we have not been looking at the results in the high current density region, and there is no need for validation test in this region. However, it is seen from Fig. 2 that the end section of the polarization curve (the concentration losses section) differs only slightly from the experimental data whereas the difference is greater in higher current densities.

8.2 General Study of Variables in the PEMFC

Figure 3 shows average convection velocity contour of gas species in the computational domain. The order of fluid velocity in the membrane is a few order of magnitude lower than velocity in the channel. Porous GDL behaves like a wall in which gases are entered mostly by diffusion phenomenon. Due to higher entrance velocity in cathode channels, the velocity alongside the channel also remains higher. By development of boundary layer in the walls, the velocity in the middle of channels along the channel direction will increase. Air contains of 80% nitrogen. This substance helps air to maintain the enough momentum to drain the water plug. Reduction of gas flow rate inside the anode channel is due the lake of carrier gas such as nitrogen (Lee and Bae 2012), it is probable that the anode is flooded.

In Fig. 4, streamlines are shown in the computational domain. Streamlines in GDL shows that in both cathode and anode, the average flow direction is from gas channel to GDL and thus to the membrane and velocity order in GDL is much lower than in the channel. The reason for having many lines in the membrane is the point that some of the species are consumed there. Another reason is the fact that velocity order in the membrane is low, thus round-off error occurs as a result.

Figure 5 shows saturated liquid water contour (*s*) in the computational domain of the base case. Due to high convection velocities in channels, the liquid cannot condense, and the amount of produced liquid water in GDL is transferred in a narrow distance at

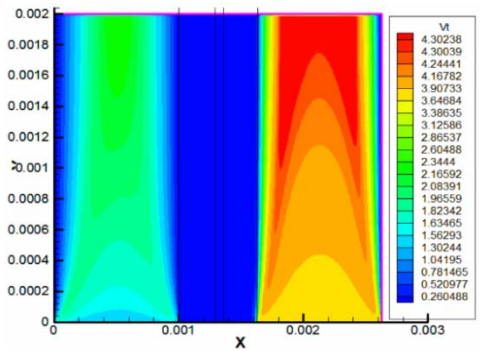

Fig. 3. Convection velocity contour

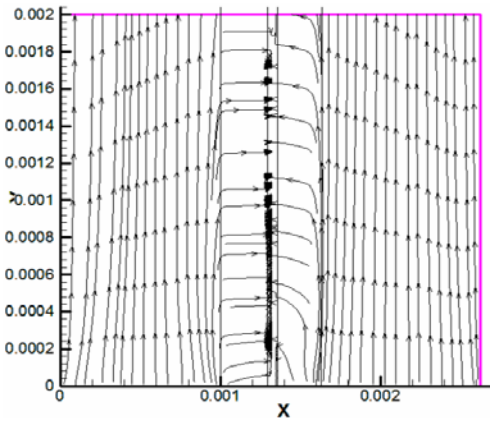

Fig. 4. Convection streamlines

the boundary between GDL and channel, and as a result, saturation in channels is very low. Thus, there is no liquid water in the membrane, and liquid water in the membrane is assumed to be dissolved. Amount of liquid water in the cathode is more than the anode. In the initial part of the channel due to the higher level of reaction and water production, liquid water is more, which this amount is decreased in the channel direction. Usually, in PEMFC, liquid water is mainly formed on the cathode side, and most of the water management studies are done on the cathode side.

Figure 6 shows temperature distribution in the computational domain. The hydrogen oxidation in the anode is an endothermic reaction, while the oxygen reduction at the cathode is an exothermic reaction. Considering this, the anode temperature is lower than the temperature of the cathode, and as a result, the anode flooding is more intense due to the distillation of liquid water from the cathode. Increasing the temperature of the anode plate is moderate, an effective way to reduce its flooding.

Figure 7 shows mole concentration contour of hydrogen, oxygen, water vapor and dissolved water in polymer phase. It can be seen from Fig. 7-a that hydrogen diffuses to the cell depth from anode channel boundaries and reaches the CL. A discontinuity is observed in the distribution of hydrogen concentration in CL boundary since hydrogen must be dissolved in water in order to

enter the membrane. Hydrogen mole concentration

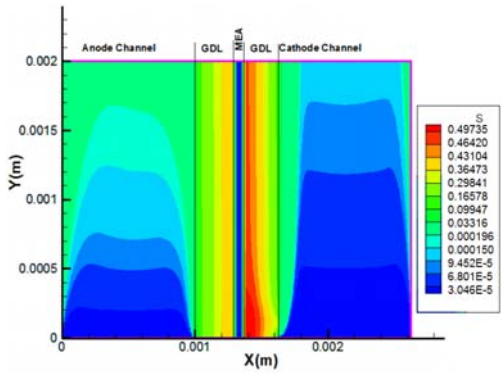

Fig. 5. Saturated liquid water (s) contour

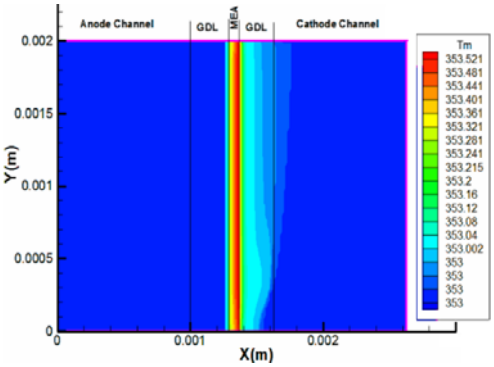

Fig. 6. Temperature contour

in the membrane is much lower than its concentration in the channel. Only a small amount of hydrogen can cross the membrane and reach the cathode CL and is consumed by direct reaction with oxygen. It is seen that, in the anode channel direction, the hydrogen concentration is decreased by its consumption. The closer it gets from anode channel to anode catalyst, hydrogen concentration will decrease again. Based on Fig. 7-b, on the cathode side of the membrane, where oxygen converts from free form to dissolved form, apparent discontinuity is distinguishable. Similar to hydrogen, a small amount of oxygen crosses the membrane and in the anode CL reacts with hydrogen (Seddiq *et al*. 2006). It is observed that in the cathode channel direction, the oxygen concentration is decreased by its consumption. When it gets closer from channel to the cathode CL, the oxygen concentration will decrease again. Based on Fig. 7-c, mole concentration of dissolved water in the polymer phase is almost one, and part of the dissolved gases also remain in the membrane. Water vapor in cathode GDL is more than anode side due to water generation. Since the velocity of input flow in cathode channel is higher, the amount of water diffusion to the cathode channel is lower than anode channel. It is observed that, in the direction of channels, mole concentration of water vapor is increased by the water production. At the locations closer to the related CL, the mole concentration of the water vapor is larger. This is due to the decreased mole concentration of reactant materials, which results in the increased mole concentration of water vapor. Water transfer due to electro-osmotic drag can be a reason for the higher level of water vapor in cathode GDL.

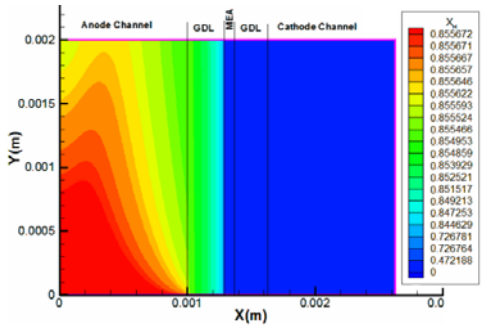

(a)

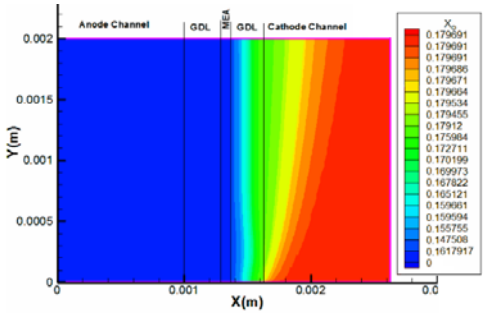

(b)

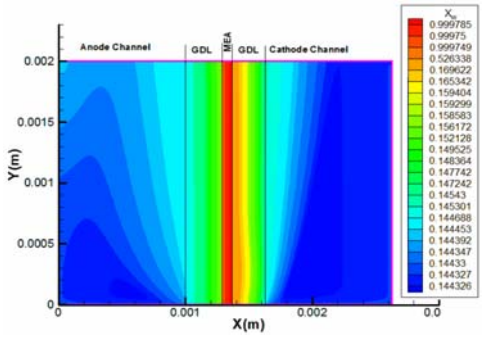

(c)

Fig. 7. Mole concentration contour: a) Hydrogen; b) Oxygen; c) Water vapor and dissolved water

8.3 Effect of Including Liquid Water Transfer on PEMFC Performance

In Figs. 8-a and 8-b, polarization curve and efficiency curve of the model for the base case including and excluding liquid water, are shown. As it is obvious from the curves, when the effect of liquid water on PEMFC is considered, related polarization curve will decrease. Liquid water affects the cell efficiency in two ways. One of them is the effect of mass transfer by blocking gases passage in GDL that affects diffusivity equations. Another effect of liquid water is on CL surface that causes to decrease its effective surface. The lower the current density, the closer to each other the polarization curves. The reason for this phenomenon is that in low current densities, lower liquid water is produced. Thus, both of the above-mentioned loss effects will

decrease. The Trend of curve change in Fig. 8-b is completely similar to polarization curve where similar effects are visible.

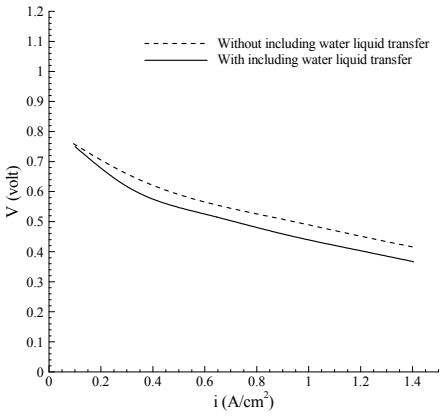

(a)

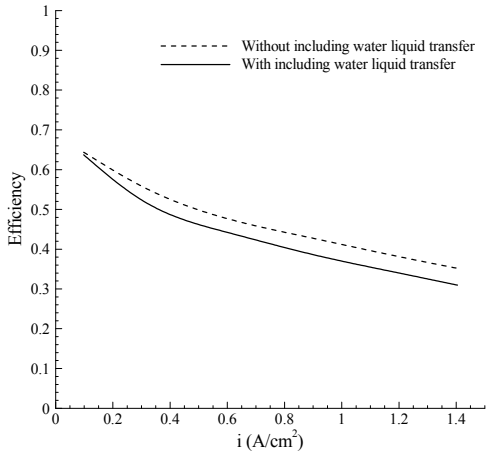

(b)

Fig. 8. Effect of considering the water liquid transfer on a) Polarization curve; b) Efficiency curve

8.4 Investigation of the Effects of Parameters on PEMFC Performance

For all of the results in this section, cell condition is taken as the base case (see Table 6), and only one of the variables is changed.

8.4.1 Effect of Water Diffusivity

Effect of liquid water diffusivity on the distribution of liquid water saturation is shown in Fig. 9. This distribution is shown in the middle of the channel (y=1.0 mm). Liquid water diffusivity is changed due to different factors including hydrophilicity or hydrophobicity of GDL. As it is shown in the Fig. 10, if liquid water diffusivity is increased (increasing the GDL hydrophobicity), then liquid water transfer will also increase and therefore, lower water liquid accumulates in GDL and cell efficiency will increase. It is understood from the curve that the maximum water level in the base condition is around 0.47. This amount is decreased to 0.31 by doubling the liquid water diffusivity and is increased to 0.68 by decreasing the liquid water diffusivity to half of its value. It is observed that liquid water on the cathode side is more than anode and by moving from channel to CL, its value will increase. Liquid water content, in the membrane, is zero. The amount of saturated liquid water at the anode electrode suggests a need for further investigation of liquid water behavior in this electrode.

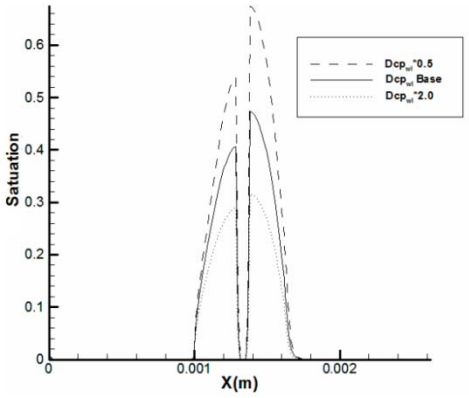

Fig. 9. Distribution of saturated liquid water in different liquid water diffusivity

Figure 9 clearly identifies the importance of unified PEMFC simulation by considering the anode electrode in the structure of the cell. It can be seen that increasing the mass diffusivity in the anode electrode helps to reduce water accumulation. If a hydrophilic GDL is used at the anode, this GDL can wick liquid water accumulated in the anode GFC and therefore, a smaller amount of water flooding will be observed under similar operating conditions. The other cause of the flooding in the anode is back diffusion from cathode to anode due to the difference in the concentration of liquid water in the two electrodes, which occurs with increasing water saturation in the cell

8.4.2 Effect of Current Density

In Fig. 10, distribution of liquid water saturation is shown in the vertical direction of the membrane (x) at the middle of the channel (y=1.0 mm), with three different current densities. In the current density of 0.1 Acm^{-2}, the saturation level of liquid water is very low, and its maximum level is around 0.05, but in current densities of 0.6Acm^{-2}, and 1.18Acm^{-2}, the maximum water saturation level is 0.44 and 0.47, respectively. It is observed that the higher the consumption current, the more the produced liquid water and thus the activation voltage will increase and the cell voltage will decrease. In other words, the current density is a control parameter for the formation of water in both electrodes. The high current density results in a greater flux of water from the anode to the cathode by electroosmotic drag, reducing the water content in the anode and reducing the tendency to form liquid water. On the other hand, increasing the current density causes back diffusion from the cathode to the anode. These two factors, together with the pressure difference between two electrodes, are effective in anode flooding. The results of Fig. 10 show that, as the current density increases, the amount of water in the anode is also increased.

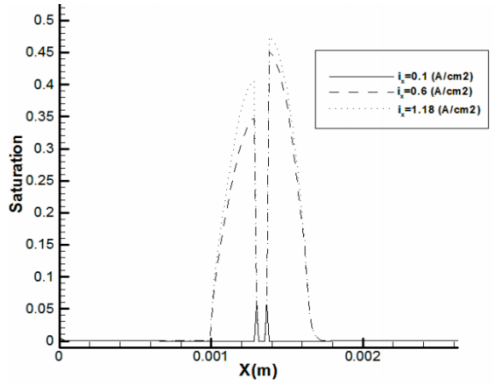

Fig. 10. Distribution of saturated liquid water in different current densities

8.4.3 Effect of Membrane Thickness

Effect of membrane thickness on a few variables at current density i=1.18 Acm^{-2} is shown in Table 8. Membrane thickness has a little effect on oxygen concentration. Table 5 shows that the difference of concentrations is almost 0.07, which causes a change of around 0.5% in concentration. Since thickness affects ohmic voltage loss directly, cell power will decrease based on membrane thickness increase. According to Table 5, this decline is between 10% to 20%. Since ohmic voltage loss has a direct relation with current density, in higher current densities, the effect of membrane thickness on power density decrease will be more. Probably due to enough current density increase, the value of power density after passing a maximum point reaches zero value because the ohmic voltage loss also increases. By the increase of membrane thickness, ohmic loss and produced heat caused by it are both increased, and the liquid temperature rises. So as it is shown in Table 8, cell temperature is increased by the increase of membrane thickness. It seems that ohmic loss, which means an increase of barrier against proton movement, results in the decreased reaction rate. This issue is observable from data of Table 8. The Increase of membrane thickness results in a decline in gas passing and cross-over phenomenon because the barrier against gas passing becomes greater. The increased trend of crossover efficiency, by an increase of membrane thickness, is shown in Table 8. High cross-over efficiency means more non-permeable membrane and lower gas passing loss.

Table 8 Effect of membrane thickness on a few variables

Membrane thickness (µm)	50.8	108	230
Power density (W/m)	10.73	9.77	7.83
Minimum of oxygen mole concentration (mole m^{-3})	14.79	14.85	14.93
Maximum of cell temperature (K)	353.56	353.63	353.78
Maximum of liquid water saturation	0.531	0.529	0.527
Cross-over efficiency	0.992	0.997	0.999
Overall efficiency	0.385	0.351	0.281
Potential (V)	0.455	0.414	0.332
Ohmic potential loss (V)	0.0496	0.0902	0.1720

8.4.4 Effects of Oxygen to Nitrogen Ratio

The effect of oxygen to nitrogen ratio for some variables in the current density i=1.18 Acm^{-2} is shown in Table 9. Table 9 is presented for three values of oxygen to nitrogen ratio in which 0.266 is for air mixture and infinity is for pure oxygen and 0.15 is for oxygen level lower than normal level. It is obvious that by increasing the oxygen level in the channel entrance, the minimum oxygen mole concentration in the whole computational domain will increase. By increase of oxygen level, decrease of activation potential loss will occur. It results in an increase of cell potential, cell total efficiency and power density. The Decrease of activation potential loss results in the decreased heat produced by this potential loss. Thus, by an increase of oxygen concentration, cell temperature slightly will decrease which this decrease is trivial because of the short length of the channel and low concentration of the reactants at the reaction sites. The higher the difference between the concentrations of both sides of the membrane, the more the fluid transfers due to cross-over phenomenon. Therefore, by an increase of oxygen concentration, crossover efficiency will decrease and thus more oxygen is consumed on the anode side without producing electricity.

Table 9. Effect of oxygen to nitrogen ratio for some variables at i=1.18 Acm-2

Oxygen to nitrogen ratio	0.15	0.266	Infinite (Pure oxygen)
Power density (W/m)	8.751	9.553	14.070
Minimum of oxygen mole concentration (mole m^{-3})	7.671	14.785	85.840
Maximum of cell temperature (K)	353.641	353.602	353.458
Maximum of liquid water saturation	0.530	0.531	0.534
Cross-over efficiency	0.994	0.992	0.981
Overall efficiency	0.315	0.343	0.499
Potential (V)	0.371	0.405	0.596
Ohmic potential loss (V)	0.0495	0.0495	0.0496

8.5 Cross-over Phenomenon Investigation

In Fig. 11, the trend of change in the cross-over efficiency (permeability efficiency) against the current density in the base condition is shown and compared with results of Seddiq *et al.* (2004) which studied the phenomenon of cross-over without accounting for the liquid water.

It is observed that by increasing current density, the ratio between the gases passing through the membrane to the gasses which are consumed in the reaction is reduced. Thus, permeability efficiency will increase, and the losses caused by the direct reaction will decrease. When the higher current is exerted from the cell, the reactants consumption is increased, and their concentration in the related CL will also decrease. Due to this reason, lower levels of reactants are diffused to the other side of the cell in order to make a direct reaction on the opposite side of the cell.

As it can be seen in Fig. 11, when the effect of liquid water on PEMFC is considered, the cross-

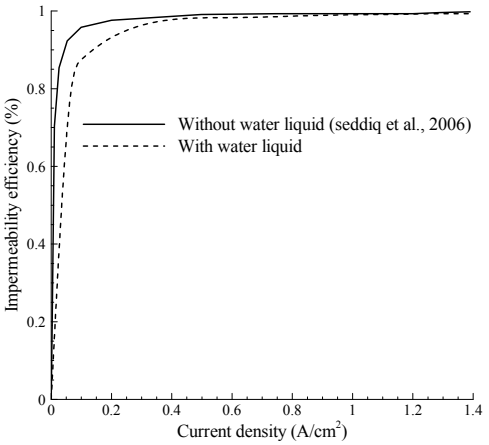

Fig. 11 Cross-over efficiency curve

over efficiency curve will decrease. One effect of the liquid water is the blockages of the GDL passages against the gases. Based on Fig. 12, at the current density of 0.1 A/cm^2, cross-over effect causes about 12% reduction in cell efficiency. This amount is about 4% in the case where the transfer of water is not considered. By decreasing the current density, this effect is increased. This result implies that considering the transfer of water in the study of the cross-over phenomenon is of real importance.

9. CONCLUSION

In the present paper, the liquid water transfer and gas cross-over through the membrane were investigated. In almost all other works, the membrane has been considered impermeable to oxygen, hydrogen and nitrogen gases. Moreover, the studies of water management have mostly focused on the cathode side since the occurrence of flooding is more probable in this region. However, experimental studies have revealed that flooding can also occur in the anode GFC in special working conditions. The transfer of liquid water was considered both in the cathode and anode sides, and the following important results were accomplished:

1) Considering the transfer of water in the study of the cross-over phenomenon is important. At the current density of 0.1 A/cm^2, cross-over effect causes about 12% reduction in cell efficiency, while this amount is about 4% in the case where the transfer of water is not considered. By decreasing the current density this effect increases.

2) The amount of water saturation at the anode GDL is considerably significant (The amount of liquid water in the cathode is more than anode) and water content in both electrodes are increased with increasing current density. At the current density 0.1 Acm^{-2} maximum level of liquid water is around 0.05, but in current densities of 0.6Acm^{-2}, and 1.18Acm^{-2}, the maximum water saturation level is 0.44 and 0.47, respectively.

3) The Increase of anode electrode temperature and flow rate in the anode gas channels are two solutions for a decrease of flooding in this electrode.

4) Choosing a more hydrophobic GDL for the cathode and a more hydrophilic GDL for anode will increase the efficiency of the cell. The maximum saturated water level in the base condition is around 0.47. This amount is decreased to 0.31 by doubling the liquid water diffusivity and is increased to 0.68 by decreasing the liquid water diffusivity to half of its value.

5) Transfer of species especially in the GDL has an important influence on the cell efficiency. The Decrease of GDL thickness, an increase of its porosity and decrease of its tortuosity will reduce the loss of species concentration besides CL.

6) The increase of membrane thickness will result in a decrease of gas cross-over through the membrane. At low current density, consideration of the permeability efficiency is essential.

Liquid water affects the cell efficiency in two ways. First of all, it blocks the reactant gas pass; secondly, it causes a decrease in the effective catalyst area. Based on the results of this research we can manage formation and transfer of liquid water in cathode and anode by parameters such as current density, temperature, hydrophobic GDL/ hydrophilic GDL and flow rate change. This research shows the importance of more studies in the field of two-phase flows and water management in the PEMFC anode by using algorithms which take into account the movement of drops in the channel. By considering the dynamics of drops in the anode gas channel, we can certainly propose more precise solutions for water management. This issue is being investigated by the writers of this paper and will be published in the near future.

ACKNOWLEDGEMENTS

This work is supported by Tarbiat Modares University (TMU). The authors are thankful to Mr. Peyman Havaej and also Dr. Mohammad Reza Safaei for their helps.

REFERENCES:

Anderson, M., Beale, S. B., Espinoza, M., Wu, Z. and Lehnert, W. (2016). A review of cell-scale multiphase flow modeling, including water management, in polymer electrolyte fuel cells, *Applied Energy* 180, 757–778.

Anderson, R., Zhang, L., Ding, Y., Blanco, M., Bi, X. and Wilkinson, D.P. (2010). A critical review of two-phase flow in gas flow channels of proton exchange membrane fuel cells, *Journal of Power Sources* 195, 4531-4553.

Ashrafi, M. and Shams, M., (2017). The e□ects of flow-field orientation on water management in PEM fuel cells with serpentine channels, *Applied Energy* 208, 1083-1096.

Bernardi, D. M. and Verbrugge, M. W. (1992). A

Mathematical Model of the Solid- Polymer-Electrolyte Fuel Cell, *Journal of The Electrochemical Society* 139, 2477-2491.

Cai, Y., Yang, T., Sui, P. C. and Xiao, J. (2016) A numerical investigation on the effects of water inlet location and channel surface properties on water transport in PEMFC cathode channels, *International journal of hydrogen energy* 41 , 16220-16229.

Djilali, N. (2007). Computational modelling of polymer electrolyte membrane (PEM) fuel cells: Challenges and opportunities, *Energy* 32, 269-280.

Ferreira, R. B., Falcão, D. S., Oliveira, V. B. and Pinto, A.M.F.R. (2015). Numerical simulations of two-phase flow in an anode gas channel of a proton exchange membrane fuel cell, *Energy* 82, 619-628.

Ferreira, R. B., Falcão, D. S., Oliveira, V. B. and Pinto, A.M.F.R. (2015). Numerical simulations of two-phase flow in proton exchange membrane fuel cells using the volume of fluid method – A review, *Journal of Power Sources* 277, 329-342.

Ge, S. and Wang, C. Y. (2007). Liquid water formation and transport in the PEFC anode, *Journal of The Electrochemical Society* 154, B998-B1005.

Gurau, V., Liu, H. and Kakaç, S. (1998). Two-dimensional model for proton exchange membrane fuel cells, *AIChE Journal* 44, 2410-2422.

Hou, Y., Zhang, G., Qin, Y., Du, Q. and Jiao, K. (2017). Numerical simulation of gas liquid two-phase flow in anode channel of low-temperature fuel cells, *International Journal of Hydrogen Energy* 42, 3250-3258.

Hu, M., Gu, A., Wang, M., Zhu, X. and Yu, L. (2004). Three dimensional, two phase flow mathematical model for PEM fuel cell: Part I. Model development, *Energy Conversion and Management* 45, 1861-1882.

Hwang, J. J. (2007). A complete two-phase model of a porous cathode of a PEM fuel cell, *Journal of Power Sources* 164, 174-181.

Lee, D. and Bae, J. (2012). Visualization of flooding in a single cell and stacks by using a newly-designed transparent PEMFC, *International Journal of Hydrogen Energy* 37, 422-435.

Meng, H. (2007). A two-phase non-isothermal mixed-domain PEM fuel cell model and its application to two-dimensional simulations, *Journal of Power Sources* 168, 218-228.

Natarajan, D. and Van Nguyen, T. (2001). A two-dimensional, two-phase, multicomponent, transient model for the cathode of a proton exchange membrane fuel cell using conventional gas distributors, *Journal of The Electrochemical Society* 148, A1324-A1335.

Pasaogullari, U. and Wang, C. Y. (2004). Two-phase transport and the role of micro-porous layer in polymer electrolyte fuel cells, *Electrochimica Acta* 49, 4359-4369.

Pasaogullari, U. and Wang, C. Y. (2005). Two-phase modeling and flooding prediction of polymer electrolyte fuel cells, *Journal of The Electrochemical Society* 152, A380-A390.

Rajan, A., Garg, A., Vijayaraghavan, V., Kuang, Y. C., Ooi, M. P. ,(2018) Parameter optimization of polymer electrolyte membrane fuel cell using moment-based uncertainty evaluation technique, *Journal of Energy Storage* 15, 8-16.

Seddiq, M., Khaleghi H. and Mirzaei, M. (2006). Numerical analysis of gas cross-over through the membrane in a proton exchange membrane fuel cell, *Journal of Power Sources* 161, 371-379.

Sergi, J. M. and Kandlikar, S. G. (2011). Quantification and characterization of water coverage in PEMFC gas channels using simultaneous anode and cathode visualization and image processing, *International Journal of Hydrogen Energy* 36, 12381-12392.

Siegel, C. (2008). Review of computational heat and mass transfer modeling in polymer-electrolyte-membrane (PEM) fuel cells, *Energy* 33, 1331-1352.

Siegel, N. P. (2003). Development and validation of a computational model for a proton exchange membrane fuel cell, PhD thesis, Virginia Polytechnic Institute and State University.

Siegel, N. P., Ellis, M. W., Nelson, D. J. and von Spakovsky, M.R. (2003). Single domain PEMFC model based on agglomerate catalyst geometry, *Journal of Power Sources* 115, 81-89.

Siegel, N. P., Ellis, M. W., Nelson, D. J. and von Spakovsky, M.R. (2004). A two-dimensional computational model of a PEMFC with liquid water transport, *Journal of Power Sources* 128, 173-184.

Song, G. H. and Meng, H. (2013). Numerical modeling and simulation of PEM fuel cells: Progress and perspective, *Acta Mechanica Sinica* 29, 318-334.

Springer, T. E., Zawodzinski, T. A. and Gottesfeld, S. (1991). Polymer electrolyte fuel cell model, *Journal of The Electrochemical Society* 138, 2334-2342.

Um, S., Wang, C. Y. and Chen, K. S. (2000). Computational fluid dynamics modeling of proton exchange membrane fuel cells, *Journal of The Electrochemical Society* 147, 4485-4493.

Wang, L., Husar, A., Zhou, T., Liu, H. (2003). A parametric study of PEM fuel cell performances, *International Journal of Hydrogen Energy* 28, 1263–1272.

Weber, A. Z., Borup, R. L., Darling, R. M., Das, P.

K., Dursch, T. J., Gu, W., Harvey, D., Kusoglu, A., Litster, S., Mench, M. M., Mukundan, R., Owejan, J. P., Pharoah, J. G., Secanell, M. and Zenyuk, I. V. (2014). A Critical Review of Modeling Transport Phenomena in Polymer-Electrolyte Fuel Cells, *Journal of The Electrochemical Society* 161, F1254-F1299.

Xing, L., Du, S., Chen, R., Mamlouk M. and Scott, K. (2016). Anode partial flooding modelling of proton exchange membrane fuel cells: Model development and validation, *Energy* 96, 80-95.

Zhang, G., Fan, L., Sun, J. and Jiao, K. (2017). A 3D model of PEMFC considering detailed multiphase flow and anisotropic transport properties, *International Journal of Heat and Mass Transfer*, 115, 714–724.